Dynamical reconstruction of the exciton in LiF with inelastic x-ray scattering

Peter Abbamonte[†‡], Tim Graber[§], James P. Reed[†], Serban Smadici[†] Chen-Lin Yeh[¶], Abhay Shukla[‖], Jean-Pascal Rueff[††], and Wei Ku[‡‡]

[†]Department of Physics and Frederick Seitz Materials Research Laboratory, University of Illinois, 104 South Goodwin Avenue, Urbana, IL 61801; [§]Center for Advanced Radiation Sources, University of Chicago, Chicago, IL 60637; [¶]Department of Physics, Tamkang University, Tamsui, Taiwan 25137, Taiwan; [‖]Unité Mixte de Recherche 7590, Université Pierre et Marie Curie, F-75005 Paris, France; [††]Synchrotron SOLIEL, L'Orme des Merisiers, BP-48 Saint Aubin, 91192 Gif-sur-Yvette, France; and [‡‡]Department of Physics, Building 510, Brookhaven National Laboratory, Upton, NY 11973

Edited by Esther M. Conwell, University of Rochester, Rochester, NY, and approved June 6, 2008 (received for review February 23, 2008)

The absorption of light by materials proceeds through the formation of excitons, which are states in which an excited electron is bound to the valence hole it vacated. Understanding the structure and dynamics of excitons is important, for example, for developing technologies for light-emitting diodes or solar energy conversion. However, there has never been an experimental means to study the time-dependent structure of excitons directly. Here, we use causality-inverted inelastic x-ray scattering (IXS) to image the charge-transfer exciton in the prototype insulator LiF, with resolutions $\Delta t = 20.67$ as (2.067×10^{-17} s) in time and $\Delta x = 0.533$ Å (5.33×10^{-11} m) in space. Our results show that the exciton has a modulated internal structure and is coherently delocalized over two unit cells of the LiF crystal (≈8 Å). This structure changes only modestly during the course of its life, which establishes it unambiguously as a Frenkel exciton and thus amenable to a simplified theoretical description. Our results resolve an old controversy about excitons in the alkali halides and demonstrate the utility of IXS for imaging attosecond electron dynamics in condensed matter.

attoscience | Wannier function

Excitons are frequently said to come in two types (1). The first are the weakly bound Wannier excitons (2) that occur in semiconductors like Ge and Cu_2O. These excitations are delocalized and can be described as an electron and a hole orbiting one another in a dielectric background. The second are the tightly bound Frenkel excitons (3) that occur, for example, in solid noble gases or organic molecular crystals. These excitations are highly localized and normally described in terms of atomic wave functions on a single-lattice site.

The first materials in which excitons were observed experimentally (4) were the alkali halides, such as NaCl, KBr, and LiF, and it has long been believed that they are intermediate between the Frenkel and Wannier limits (1, 4, 5). These excitons are strongly bound but are of the "charge transfer" (CT) type, meaning they involve transfer of an electron from an alkaline *p* to a halogen *s* level, so cannot be described as atomic orbitals on a single atom. This might seem to imply that CT excitons are not amenable to either a Wannier or Frenkel description.

Long ago, many authors attempted to describe the nonlocality of CT excitons theoretically. Overhauser (6) introduced the "electron transfer" model, which correctly accounted for the symmetry and multiplicity of states but relied on pure atomic orbitals resulting in unrealistic binding energies. Later, Dexter proposed an "excitation model" (7) in which atomic wave functions are corrected with an envelope function, although this envelope had to be unphysically rapidly varying. Eventually, Hopfield (8) argued that a Wannier model is the best description. This debate was a fundamental one, over how to properly describe corrections to the self-consistent field concept in condensed matter. It was never resolved, however, partly because of insufficient information about the internal structure and dynamics of the exciton.

This issue has since been addressed by modern *ab initio* methods (9). These methods first use density functional theory (10) to compute the electron band structure, and then employ a correction for interactions (the so-called "GW" correction). The output wave functions are then used as a basis for solving the Bethe–Salpeter equation for the two-electron Green's function (9, 11–13), which can readily be used to compute optical spectra. This approach has achieved impressive agreement with experiment (9), but it is very computationally expensive and not easily scalable to large systems. There is therefore still a need for a simple description, in the vein sought by early authors, that can account approximately but accurately for the nonlocal properties of the exciton. To formulate such a description, experimental data on the structure and dynamics of the exciton is key.

For this purpose, we have studied the valence, CT exciton in the prototypical alkali halide LiF with causality-inverted inelastic x-ray scattering (IXS) (14). IXS measures the dynamic structure factor, $S(\mathbf{k}, \omega)$ (15), which at zero temperature is the imaginary part of the Fourier transform of the retarded density–density propagator, $\chi(\mathbf{x}, t) = -i/\hbar < 0|\delta\hat{n}(\mathbf{x}, t)\delta\hat{n}(0, 0)|0 > \theta(t)$, where $\delta\hat{n}(\mathbf{x}, t)$ is an operator for the induced electron density. $\chi(\mathbf{x}, t)$ describes the probability that a point disturbance in the electron density will travel a distance $\mathbf{x}$ after elapsed time t. We recently demonstrated a method by which $\chi(\mathbf{x}, t)$ can be reconstructed explicitly from experimental data by imposing causality as a constraint (14). This method allows many-electron dynamics to be imaged in real time with resolutions approaching 1 attosecond (10^{-3} fs) in time and 0.1 Å (10^{-11} m) in space.

This approach allows one to explicitly determine whether an exciton is of Frenkel, Wannier, or some intermediate type. To illustrate how, we appeal to the formalism introduced by Wannier (2), who showed that, in general, the wave function for an exciton is determined by diagonalizing the matrix

$$H_{\beta,\beta'}(\mathrm{K}) = \sum_R e^{-i\mathbf{K}\cdot\mathbf{R}} \langle \mathbf{R}, \mathbf{R} + \beta | H | 0, \beta' \rangle \qquad [1]$$

where $|\mathbf{R}, \mathbf{R} + \beta\rangle$ represents a hole in a valence band Wannier function at position $\mathbf{R}$ and an electron in the conduction band Wannier function at $\mathbf{R} + \beta$. Here, $\mathbf{K}$ is the center of mass momentum of the exciton and β, which is a Bravais lattice vector, is the electron-hole separation. For a Wannier exciton, many

Author contributions: P.A. designed research; P.A., T.G., J.P.R., S.S., C.-L.Y., A.S., and J.-P.R. performed research; P.A., C.-L.Y., A.S., and W.K. contributed new reagents/analytic tools; P.A., C.-L.Y., and W.K. analyzed data; and P.A. and W.K. wrote the paper.

The authors declare no conflict of interest.

This article is a PNAS Direct Submission.

Freely available online through the PNAS open access option.

[‡]To whom correspondence should be addressed. E-mail: abbamonte@mrl.uiuc.edu.

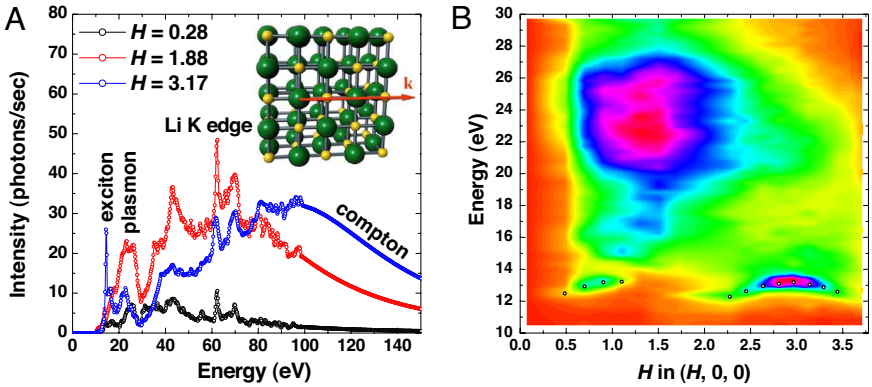

Fig. 1. Inelastic x-ray scattering data, that is, $Im[\chi(k, \omega)]$, for LiF. (*A*) Individual spectra for selected *H* values, showing the exciton line, interband transitions, the valence plasmon, core levels, and Compton scattering background. The smooth lines are Lorentzian extrapolations. (*Inset*) Crystal structure of LiF with F atoms shown in yellow and Li atoms shown in green. The red arrow denotes the direction of the experimental momentum transfer vector, **k**. (*B*) Full response up to $\omega = 30$ eV with the fit values of ω_k^0 shown as open circles.

terms with different β's are coupled and the resultant wave function highly depends on the value of **K**. For a Frenkel exciton, because the binding energy is large, the relative motion of the electron and hole is quenched and the sum is dominated by the single term $\beta = \beta' = 0$, that is,

$$H_{0,0} = \sum_R e^{-i\mathbf{K}\cdot\mathbf{R}} \langle \mathrm{R},\ \mathrm{R}|H|0,\ 0\rangle \qquad [2]$$

in which case only one pair of Wannier functions contributes, regardless of the value of **K**. As a result, when viewed via the quantity $\chi(\mathbf{x}, t)$, which couples all **K** values together, a Wannier exciton will change shape in time, whereas a Frenkel exciton will be time-independent. IXS therefore provides a direct means to determine—independent of the explicit form of *H*—what kind of simplified picture is suitable for describing CT excitons in the alkali halides.

Results and Discussion

The raw IXS data from LiF are shown in Fig. 1. Spectra were taken over the intervals $0 < \omega < 100$ eV and $(0, 0, 0) < \mathbf{k} < (3.77, 0, 0)$, where (H, K, L) are Miller indices denoting a momentum $\mathbf{q} = 2\pi(H, K, L)/a$, where $a = 4.027$ Å is the cubic lattice parameter. Three representative spectra (Fig. 1*A*) reveal, in order of increasing energy, the valence CT exciton, a continuum of interband transitions, a valence plasmon, the 2*s* core level of F, the 1*s* core level of Li, and a broad background of Compton scattering that grows as **k** is increased. LiF has three singlet CT excitons—two transverse and one longitudinal (1)—however, IXS measures only the longitudinal charge response so we see only the longitudinal exciton here. The full **k** dependence for $\omega <$ 30 eV is displayed in Fig. 1*B*.

Fig. 1 permits some immediate observations about the exciton. First, its binding energy is large, suggestive of a local character (16, 17). However, it is also dispersive, following $\omega(k) = \varepsilon_0 + 8t\cos(ka/2)$, with $\varepsilon_0 = 14.2$ eV and $t = -0.065$ eV, which is a nonlocal effect. This seems to support the old presumption (1) that this CT exciton lies between the Wannier and Frenkel limits. However, we point out that the exciton's *intensity* is also highly momentum-dependent; it is visible only around the momentum points (0.8, 0, 0) and (3, 0, 0). This intensity must also be considered when evaluating what picture is appropriate. When combined with the exciton's dispersion, it encodes the temporal dynamics we seek.

Data Inversion. We now apply the method of ref. 14 to invert from (k, ω) to (x, t) space. This requires two preparatory steps. First, the data must be analytically continued onto a continuous ω interval. This ensures that the time variable *t* is infinite, which is required for $\chi(x, t)$ to vanish at all negative times, that is, to respect causality. This was done by simple, linear interpolation. Interpolation gives rise to slope discontinuities in Im $[\chi(k, \omega)]$ that can produce an aliasing effect in the images. However, because of our good energy resolution, this has no effect in the time interval of interest.

Second, to ensure that *t* is continuous, the spectra must be extrapolated to infinite ω. In the present case this was done by appending a Lorentzian fit to the experimental data (shown in Fig. 1*A*). One then has a continuous and piecewise analytic representation of Im $[\chi(k, \omega)]$. The time evolution is then acquired by performing a Kramers–Kronig (KK) transformation, to determine $Re[\chi(k, \omega)]$, and Fourier transforming, that is,

$$\chi(x, t) = \int \frac{dk\,d\omega}{(2\pi)^2}\,\chi(k, \omega)e^{i(kx-\omega t)} \qquad [3]$$

This integral may be simplified. $\chi(x, t)$ is purely real and LiF has inversion symmetry, so $\chi(k, \omega) = \chi^*(k, -\omega)$. If a function with this symmetry also satisfies the KK relations, its Fourier transform may be written purely in terms of its imaginary part (14, 18). Eq. **3** can therefore be rewritten

$$\chi(x, t) = \begin{cases} \dfrac{1}{2\pi^2}\displaystyle\int_0^\infty d\omega\,dk\,Im[\chi(k, \omega)]\cos(kx)\sin(\omega t) & t > 0 \\ 0 & t < 0 \end{cases} \qquad [4]$$

This expression explicitly maintains the causal properties of χ, so it is the most convenient way to transform to (x, t) space.

There is a limitation implicit in our measurements and in Eq. **4**. Because the data were collected along only one direction in reciprocal space (Fig. 1*A Inset*), Eq. **4** will yield only one-dimensional projections of the induced electron density along the [1,0,0] crystal axis. One should remember, however, that the exciton is a three-dimensional object.

Nyquist Resolution. Before showing the dynamics, it is important to explain what spatial and temporal resolutions, Δx and Δt, characterize the function $\chi(x, t)$ obtained from Eq. **4**. Because the measurements take place in (k, ω) space the term "resolution" must be carefully defined. We appeal to Nyquist's sampling theorem (19), which states that, to represent a function $g(t)$ with

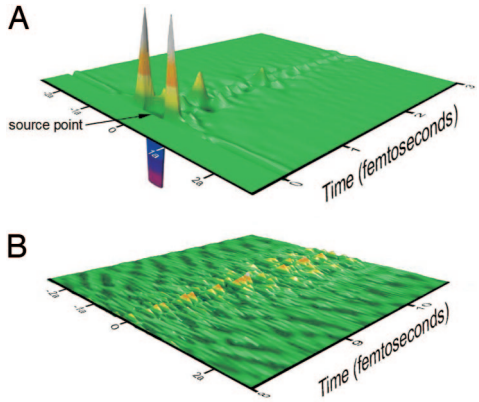

Fig. 2. Results of the full data inversion. (*A*) Complete charge response, which is an amalgam of all excitations shown in Fig. 1. The sharp, subfemtosecond features come from the Compton background and are a real-space depiction of ionization in a solid. This part of the response is sensitive to the form of the extrapolation. (*B*) Experimental noise (vertical scale expanded), which occurs by propagating the experimental noise in Fig. 1 through our inversion procedure.

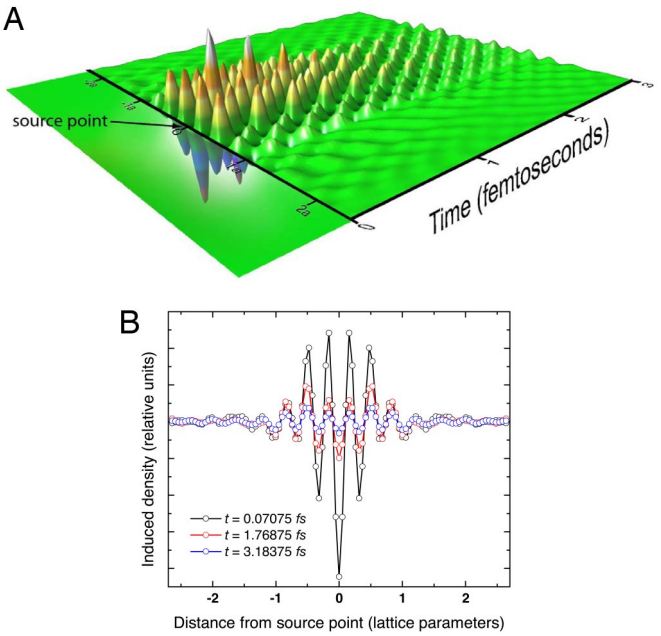

Fig. 3. Isolated exciton dynamics. (*A*) Exciton response, $\chi_e(x, t)$, for $0 < t < 3$ fs. The exciton is periodic in both space and time. (*B*) Cross-sections of the exciton at selected times, showing that its basic size and internal structure are unchanged during its life. The slight ''broadening'' at late times is a result of center-of-mass recoil.

good fidelity, it must be sampled with frequency $\omega_N = 2\omega_{\max}$, where $\omega_{\max}$ is the highest frequency present in the power spectrum of g. Stated in reverse, if we measure a Fourier spectrum out to a cutoff $\omega_{\max}$, this is equivalent to sampling it with resolution $\Delta t = \pi/\omega_{\max}$. By this definition, the resolutions in the current measurements, which we will call "Nyquist resolutions," are $\Delta t_N = \pi/100$ eV = 20.67 as and $\Delta x_N = \pi/5.892$ Å^{-1} = 0.533 Å.

Full Dynamics. An inversion of the full dataset, taken with integration step sizes $\Delta\omega = 0.2$ eV and $\Delta k = 0.264(2\pi/a)$, is shown in Fig. 2*A*. The evolution exhibits a fast, off-scale charge response that lasts ≈200 as, followed by a series of slower oscillations. The fast response comes from the Compton scattering background and is a real space depiction of ionization in a solid. This part of the response is very sensitive to the form of the extrapolation so we do not attempt to draw any quantitative conclusions from it. The slower features, which are present starting from $t \approx 70$ as and have a lifetime of several femtoseconds, are an amalgam of phenomena including the CT exciton, interband processes, plasmon oscillations, and core transitions. The experimental noise level is shown in Fig. 2*B*.

This image demonstrates the inversion procedure, but contains too many interleaved processes to draw conclusions about specific excitations. To address the exciton, it must be isolated from the other parts of the response.

Exciton Dynamics. The exciton may be isolated by realizing that our inversion procedure is *linear*. That is, if one arbitrarily divides the spectra into two parts, $Im[\chi(k, \omega)] = Im[\chi_1(k, \omega)] + Im[\chi_2(k, \omega)]$, it is necessarily true that $Im[\chi(x, t)] = Im[\chi_1(x, t)] + Im[\chi_2(x, t)]$. Further, the exciton lies below the band edge, that is, it does not overlap other excitations in energy. Through straightforward data fitting, described in detail in *Methods*, we can divide the response into exciton processes, $Im[\chi_e(k, \omega)]$, and nonexciton processes, $Im[\chi_{ne}(k, \omega)]$. Inversion of the former will reveal the dynamics of the exciton.

The time evolution of the CT exciton is shown in Fig. 3*A*. It rises to its full amplitude in ≈70 as, and then oscillates with an average period of 283 as. The exciton is coherently delocalized over approximately two lattice sites, that is, four Li–F bonds. Interestingly, its internal structure is seen to be oscillatory with period of $a/3$, which is an outcome of the intense scattering near (3, 0, 0). The exciton decays below the noise level after ≈5 fs.

Cross-sections of the exciton at selected times are plotted in Fig. 3*B*. During the course of its life the exciton never leaves the two-unit-cell region it occupies at $t = 70$ as and maintains its basic $a/3$ internal periodicity. One might have expected significant shape changes, given the exciton's dispersion, but this effect is tempered by the k-dependence of its intensity. That the CT exciton's structure is rigid is evidence that its wave function is dominated by a small number of terms, that is, is described by Eq. **2** and is well characterized by a Frenkel model.

If correct, this conclusion is significant because it suggests, contrary to the assumptions of refs. 1–7, a Frenkel exciton can exist in an ionic insulator, even though it involves charge transfer between multiple sites. Further, it suggests that the exciton is amenable to simpler description than the first-principles method of ref. 9. It also explains past success applying Wannier function analysis to excitons in NiO and CoO (27). To be sure of this conclusion, however, a comparison with specific Wannier functions for LiF is needed.

Comparison with Wannier Functions. To test our conclusion we performed a first-principles band structure calculation for LiF in the local density approximation (shown in Fig. 4*A*). Wannier functions (WFs) for the valence and conduction bands were constructed according to the method described in ref. 20. F was taken to be the center atom, in which case the WFs consist of three fully occupied F 2*p* orbitals (of p_x, p_y, and p_z symmetry) characterizing the three valence bands (Fig. 4*C*), and one fully unoccupied Li 2*s* orbital characterizing the conduction band (Fig. 4*B*). Notice that the Li 2*s* WF has *s* symmetry around the F site, by construction. This set of WFs exhibits the local point group symmetry of the crystal, and allows the charge-transfer exciton to be visualized as a local excitation residing on a "super atom" encompassing both F and Li orbitals. If our conclusion that the Frenkel model applies is correct, our basis set should not need to be larger than these four orbitals.

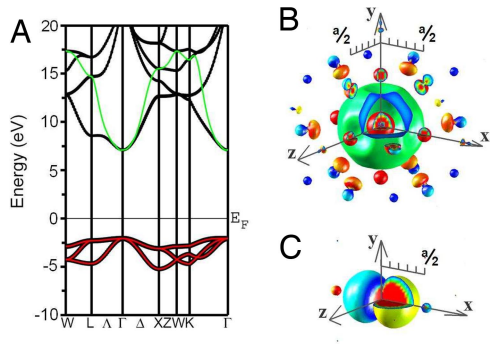

Fig. 4. Determination of the Wannier functions for LiF. (*A*) Band structure, calculated in the local density approximation. The integration region used for determining the Wannier functions is highlighted in red or green. (*B*) Constant-value surface of the Li 2*s* Wannier function for the conduction band. Notice that it has s symmetry around the F site. The color denotes the phase of the wave function. (*C*) One of the three F 2*p* Wannier functions for the valence band.

With this reduced basis set, the charge excitations can be described as a superposition of the creation of a particle in the Li 2*s* orbital, and hole in one of the F 2*p* orbitals on the same super atom. The charge susceptibility then has the form

$$\chi(\mathrm{r}_1,\, \mathrm{r}_2,\, t) = \sum_{i=x,y,z} M_i^*(r_1 - \mathrm{R}) L_i^{\mathrm{R},0}(t) M_i(\mathrm{r}_2) \qquad [5]$$

where **R** denotes the primitive unit cell that contains the vector $\mathbf{r}_1$, and the transition matrix element $M_i(\mathbf{r}) = a_{2s}^*(\mathbf{r}) a_{2p_i}(\mathbf{r})$ ($i = x, y, z$) is the product of the Wannier functions for the valence and conduction bands. The kernal $L_i^{\mathbf{R},0}(t)$ describes the probability that the exciton will propagate from the origin to unit cell **R** after elapsed time *t*.

The quantity $M_x(\mathbf{r})$, which can be thought of as the "shape" of the CT exciton in real space as seen by the x-rays, is illustrated in Fig. 5*A*. The experimental structure in Fig. 3 is a projection of this quantity onto the [1,0,0] crystal axis, broadened by the experimental resolution. Notice that both the size and internal $a/3$ periodicity are visible in this single Wannier product, in good correspondence with the experiment.

The correspondence is also clear if examined in the more traditional ($\mathbf{k}$, ω) space. In Fig. 5*B* we plot the modulus of the Fourier transform of $M_x(\mathbf{r})$, which determines the intensity (although not the energy) of the scattered x-rays at different $\mathbf{k}$ vectors. $Im[\chi(k,\, \omega)]$ determined from this matrix element is plotted in Fig. 5*C*, which should be compared with experimental Fig. 6*B*.§§ The agreement is excellent, with a single F 2*p* and Li 2*s* pair giving spectral weight at $\mathbf{k} \approx (0.8, 0, 0)$ and $\mathbf{k} \approx (3.3, 0, 0)$ as observed. The small temporal changes seen in Fig. 3*B* do not arise from mixing of other Wannier functions, but from the center of mass recoil of the exciton.

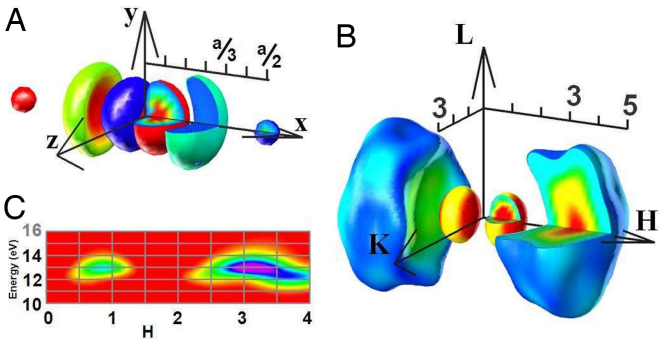

Fig. 5. Real and Fourier space images of the exciton. (*A*) Constant-value surface of the product of valence and conduction Wannier functions. The color denotes the phase of the wave function. (*B*) Structure factor. (*C*) Theoretical $Im[\chi(k, \omega)]$, for comparison with Fig. 6*B*. The intensity near $H = 1$ is reduced by 2.6 to mimic screening by the 25-eV plasmon at small *k*.

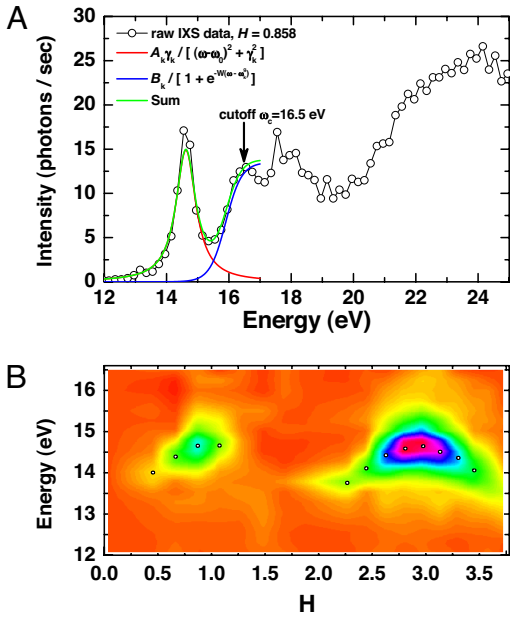

Fig. 6. Isolation of the exciton from other parts of the response. (*A*) Sample spectrum for $H = 0.858$ showing fits to the exciton and interband continuum. (*B*) Isolated exciton response, $Im[\chi_e^n(k)]$, with other processes removed. The fit values of the exciton frequency, ω_k^0, are shown as open circles. Note that the experimental noise has been carried through this procedure.

Conclusions

The rigidity of the exciton's structure, combined with the agreement between the experimental results and the Wannier analysis, leads to the conclusion that the CT exciton in LiF is decidedly Frenkel in type. This contradicts early beliefs that a CT exciton cannot be a Frenkel exciton, because it involves multiple atomic sites. The Frenkel model can still apply, as we have seen, provided one considers the exciton as residing on a super atom encompassing several sites, characterized by suitably defined Wannier functions. The only requirement for the Frenkel model to hold is that the relative motion of the electron and hole is quenched by interactions, resulting in a rigid internal structure. So the terms "CT" and "Frenkel" are not mutually exclusive.

An advantage of the Frenkel model is that it is considerably less computationally taxing than state-of-the-art *ab initio* methods (9, 11–13). Our result therefore might facilitate studies of organic molecular devices like light-emitting diodes or photocells (21, 22). Organic crystals also contain strongly bound, charge-transfer excitons (23–25) that might also be described with our generalized Frenkel model. This might permit, for example, simulations to be scaled to the dimensions of a macroscopic device.

In closing, we point out that the rapid, 70-as time scale of formation of the exciton closely resembles a recently conjectured universal attosecond response (26). Future studies of attosecond phenomena, both with IXS and with laser-based approaches,

§§The dispersion shown in Fig. 5*C*, which, like the data, follows a simple $\cos(ka/2)$ law, came from evaluating the kernel $L_i^{\mathrm{R},0}(t)$. The details of this calculation are tangential to the current article.

should determine whether the collective response of electrons exhibits such a characteristic time scale.

Methods

IXS experiments were carried out at beam lines 15-ID ChemMat CARS and 9-ID XOR at the Advanced Photon Source (APS). Scattered x-rays were energy-analyzed with a spherical, diced, Ge(444) backscattering analyzer working at an energy of 7.6 keV. Depending on the spectral region, a diamond (111) monochromator was used either alone or with a secondary Si(440) monochromator, giving an overall spectrometer resolution of either 0.52 eV or 0.13 eV, respectively. The samples were commercially obtained single crystals of the alkali halide LiF, which were lapped to 0.25-mm thickness (one absorption length) and used either in reflection or transmission geometry. After performing corrections for absorption effects, measurements in the two geometries matched well.

Isolation of the Exciton. The quantities $Im[\chi_e(k, \omega)]$ and $Im[\chi_{ne}(k, \omega)]$ were determined in the following manner. We begin with the quantity $Im[\chi(k, \omega)]$, which was experimentally sampled at frequency points ω_n, where it has the values $Im[\chi^n(k)]$. For illustration, the values $Im[\chi^n(k)]$ for a momentum $H = 0.858$ are shown in Fig. 6*A*. The data were fit up to a cutoff energy, $\omega_c = 16.5$ eV, with a Lorentzian plus a step function

$$g(\omega) = \frac{A_{\mathbf{k}}\gamma_{\mathbf{k}}^2}{(\omega - \omega_{\mathbf{k}}^0)^2 + \gamma_{\mathbf{k}}^2} + \frac{B_{\mathrm{k}}}{1 + e^{-W(\omega-\omega_{\mathbf{k}}^g)}}. \qquad [6]$$

The fit variables A_k, B_k, γ_k, ω_k^0, ω_k^g, and W may be interpreted as the intensity of the exciton, the height of the band gap edge, the width of the exciton line, the center frequency of the exciton, the size of the band gap, and the inverse width of the band edge onset, respectively. Good fits were obtained across the entire momentum range, with the case $H = 0.858$ shown for illustration in Fig. 6*A*. The values ω_k^0, which describe the dispersion of the exciton, are shown in Fig. 6*B*.

After fitting, the data were divided into two parts defined as

$$Im[\chi_e^n] = \begin{cases} Im[\chi^n] - \dfrac{B_k}{1 + \exp[-W(\omega_n - \omega_k^g)]} & \omega < \omega_c \\ 0 & \omega \geq \omega_c \end{cases} \qquad [7]$$

and

$$Im[\chi_{ne}^n] = \begin{cases} \dfrac{B_k}{1 + \exp[-W(\omega_n - \omega_k^g)]} & \omega < \omega_c \\ 0 & \omega \geq \omega_c \end{cases} \qquad [8]$$

χ_e^n describes the exciton part of the spectrum with other processes removed, and is shown in Fig. 6*B*. It was then inverted by interpolating and evaluating Eq. **4**. We note that the integrand, which for the full inversion had to be extrapolated to infinite energy, is now nonzero only over a narrow energy range. This eliminates the need to extrapolate.

ACKNOWLEDGMENTS. We thank Gerard C. L. Wong, L. Hao Tjeng, Eric L. Shirley, and Dana Dlott for helpful input. IXS measurements were supported by Department of Energy (DOE) Grant DE-FG02-07ER46459 through the Frederick Seitz Materials Research Laboratory. ChemMatCARS Sector 15 is supported by the National Science Foundation/DOE Grant CHE-0535644. Use of the Advanced Photon Source was supported by DOE Contract DE-AC02-O6CH11357. W.K. was supported by DOE Grant DE-AC02-98CH10886 and DOE-Computational Materials Science Network. C.-L.Y. was supported by NSC Grant 95-2112-M-032-001 and the Taiwanese National Science Council Research Abroad Program.

1. Knox S (1963) *Theory of Excitons* (Academic, New York).
2. Wannier GH (1937) The structure of electronic excitation levels in insulating crystals. *Phys Rev* 52:191–197.
3. Frenkel J (1931) On the transformation of light into heat in solids. I. *Phys Rev* 37:17–44.
4. Hilsch R, Pohl RW (1928) Über die ersten ultravioletten Eigenfrequenzen einiger einfacher Kristalle. *Z Physik* 48:384–396.
5. Mott NF (1938) Conduction in polar crystals. II. The conduction band and ultra-violet absorption of alkali-halide crystals. *Trans Faraday Soc* 34:500–506.
6. Overhauser AW (1956) Multiplet structure of excitons in ionic crystals. *Phys Rev* 101:1702–1712.
7. Dexter DL (1957) Exciton models in the alkali halides. *Phys Rev* 108:707–712.
8. Hopfield JJ, Worlock JM (1965) Two-quantum absorption spectrum of KI and CsI. *Phys Rev* 137:A1455–A1464.
9. Rohlfing M, Louie SG (1998) Electron-hole excitations in semiconductors and insulators. *Phys Rev Lett* 81:2312–2315.
10. Fiolhais C, Nogueira F, Marques M, eds (2003) *A Primer in Density Functional Theory* (Springer, Berlin).
11. Arnaud B, Lebegue S, Rabiller P, Alouani M (2006) Huge excitonic effects in layered hexagonal boron nitride. *Phys Rev Lett* 96:026402.
12. Hummer K, Pusching P, Sagmeister S, Ambrosch-Draxl C (2006) Ab-initio study on the exciton binding energies in organic semiconductors. *Mod Phys Lett B* 20:261–280.
13. Pederson TG (2004) Density-functional-based tight-binding calculation of excitons in conjugated polymers. *Phys Rev B* 69:075207.
14. Abbamonte P, Finkelstein KD, Collins MD, Gruner SM (2004) Imaging density disturbances in water with a 413-attosecond time resolution. *Phys Rev Lett* 92:237401.
15. van Hove L (1954) Correlations in space and time and born approximation scattering in systems of interacting particles. *Phys Rev* 95:249–262.
16. Fields JR, Gibbons PC, Schnatterly SE (1977) Electronic excitations in LiF: 10–70 eV. *Phys Rev Lett* 38:430–434.
17. Caliebe WA, Soininen JA, Shirley EL, Kao C-C, Hämäläinen K (2000) Dynamic structure factor of diamond and LiF measured using inelastic x-ray scattering *Phys Rev Lett* 84:3907–3910.
18. Madsen VA, Satchler GR (1993) Mean fields: Explicit dispersive and retardation properties of the dynamical polarization potential within a simple model *Phys Rev C* 48:1221–1231.
19. Nyquist H (1928) Certain topics in telegraph transmission theory. *Trans AIEE* 47:617–644.
20. Ku W, Rosner H, Pickett WE, Scalettar RT (2002) Insulating ferromagnetism in $La_4Ba_2Cu_2O_{10}$: An ab initio Wannier function analysis. *Phys Rev Lett* 89:167204.
21. Forrest SR (2004) The path to ubiquitous and low-cost organic electronic appliances on plastic. *Nature* 428:911–918.
22. Scholes GD, and Rumbles G (2006) Excitons in nanoscale systems *Nat. Mat.* 5:683–696.
23. Yang K, *et al.* (2007) Inelastic x-ray scattering study of exciton properties in an organic molecular crystal. *Phys Rev Lett* 98:036404.
24. Hoffmann M, *et al.* (2000) The lowest energy Frenkel and charge-transfer excitons in quasi-one-dimensional structures: Application to MePTCDI and PTCDA crystals. *Chem Phys* 258:73–96.
25. Piet JJ, *et al.* (2001) Photoexcitations of covalently bridged zinc porphyrin oligomers: Frenkel versus Wannier-Mott type excitons. *J Phys Chem B* 105:97–104.
26. Breidbach J, Cederbaum LS (2005) Universal attosecond response to the removal of an electron. *Phys Rev Lett* 94:033901.
27. Larson BC, *et al.* (2007) Nonresonant inelastic x-ray scattering and energy-resolved Wannier function investigation of d-d excitons in NiO and CoO. *Phys Rev Lett* 99:026401.